Luo *et al. Biochar* (2025) 7:117
https://doi.org/10.1007/s42773-025-00516-5

Biochar

ORIGINAL RESEARCH Open Access

Effective removal of nitrate nitrogen from water and soil using biochar-loaded nano zero-valent iron: performance and mechanisms

Lan Luo[1†], Jie Li[1†], Anina James[2], Caixia Hu[1], Guilong Zhang[1*] and Junting Pan[2*]

Abstract

Nitrogen leaching from agricultural soils serves as a main contributor to water pollution and nitrogen losses, posing significant challenges to sustainable agricultural practices. However, existing mitigation strategies often exhibit limited efficiency in reducing nitrate nitrogen (NO_3^-–N) losses and enhancing ammonium nitrogen (NH_4^+–N) retention under varying environmental conditions. To address this, our research investigated the effectiveness of biochar-supported nanoscale zero-valent iron (nZVI@BC) composites. The combination of nZVI with biochar is driven by the need to enhance biochar's adsorption capacity and provide an additional mechanism for nitrate reduction via the strong reductive properties of nZVI. Our findings indicated that nZVI@BC significantly enhanced nitrate reduction and ammonium retention compared to biochar alone, with the nZVI@BC0.6 achieving the best overall performance. The NO_3^-–N concentration in leachate was reduced by up to 71.31%, while NH_4^+–N retention increased by 53.12%, with notable improvements in nitrogen retention even in deeper soil layers. The adsorption kinetics revealed that nZVI@BC composites exhibited both rapid initial adsorption and sustained chemical reduction of NO_3^-–N, with the pseudo-second-order model verifying the dominance of chemical adsorption for nZVI-enriched treatments. The nitrate nitrogen reduction potential of nZVI@BC at various pH levels revealed optimum performance at low pH. Structural analyses (XRD, FTIR, and XPS) showed that nZVI incorporation altered the chemical environment of biochar, enhancing its surface reactivity and functional group availability, which improved nitrogen immobilization efficiency. This study highlights the potential of nZVI@BC composites, particularly nZVI@BC0.6, as an effective and sustainable strategy for mitigating nitrogen leaching, improving nitrogen use efficiency, and addressing agricultural non-point source pollution.

Highlights

- nZVI@BC enhances nitrogen retention and reduces leaching losses.
- A significant NO_3^--N reduction was achieved with nZVI@BC composites.
- nZVI@BC increases NH_4^+-N retention, improving nitrogen content.
- Fe–O and C–O functional groups enhance nitrate removal efficiency.
- nZVI@BC provides a sustainable solution for nitrogen loss mitigation.

Keywords Nitrate nitrogen, Biochar-loaded nZVI, Nitrate reduction, Leaching mitigation, Water and soil remediation

†Lan Luo and Jie Li authors contributed equally to this work.

*Correspondence:
Guilong Zhang
zhangguilong@caas.cn
Junting Pan
panjunting@caas.cn

Graphical Abstract

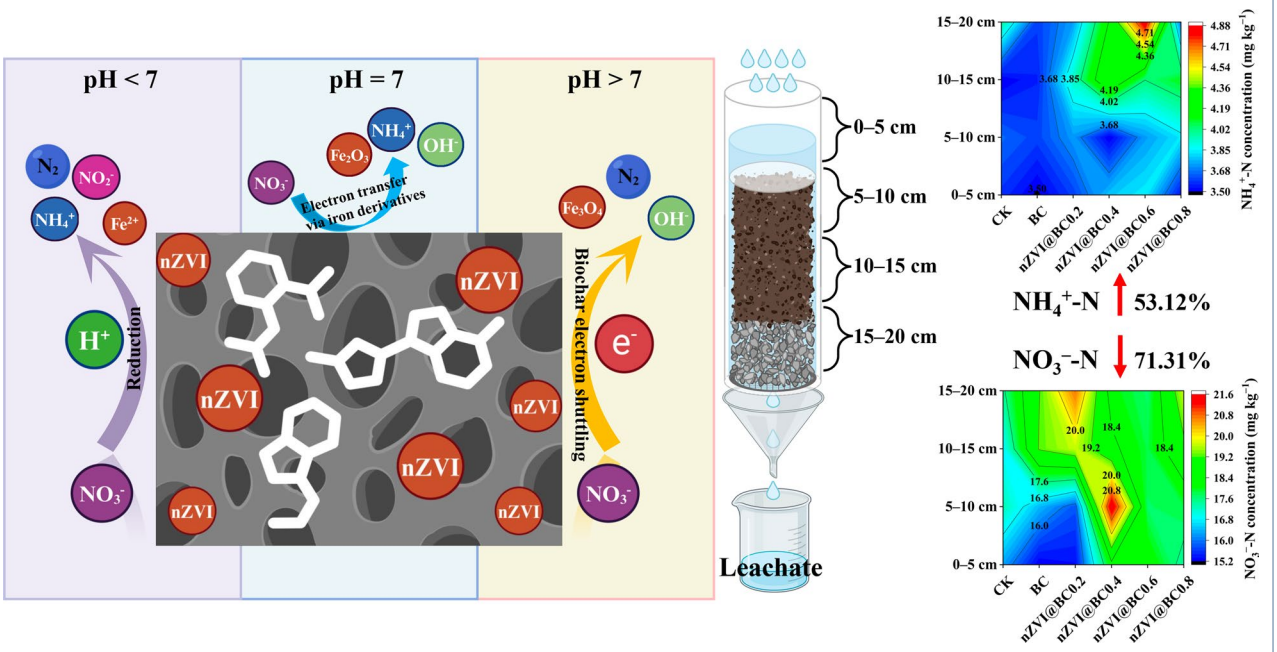

1 Introduction

Nitrogen refers to one of the most essential mineral nutrients for plants and is a key factor influencing crop yield in agricultural production (Wu et al. 2024a). Traditional fertilization methods primarily aim to increase nitrogen application to boost crop productivity (Zhang et al. 2024). Ammonium nitrogen (NH_4^+–N), an important form of nitrogen in the soil, is highly bioavailable and directly utilized by plants (Liu et al. 2025). However, due to its susceptibility to leaching and nitrification, its retention as a viable nitrogen source for plants is often compromised (Alami et al. 2025). Effective strategies to retain NH_4^+–N in the soil can significantly enhance nitrogen use efficiency (NUE), ensuring that this bioavailable nitrogen remains available for plant uptake (Li et al. 2023). On the other hand, excessive nitrogen fertilization, particularly in northern China, has led to the formation of nitrates due to the action of soil denitrifying and nitrifying microorganisms (Guo et al. 2010; Qiao et al. 2015; Zhu et al. 2022). Accumulation of nitrates formed so is enhanced by rainfall and artificial irrigation, particularly in the leaching zones of intensive agricultural regions in China (Cybulak et al. 2021; Zhu et al. 2022). High levels of nitrate nitrogen (NO_3^-–N) in the soil can lead to serious environmental issues such as groundwater contamination, soil acidification, and the disruption of soil structure, ultimately affecting soil fertility and health (Chen et al. 2010; Liu et al. 2021). Furthermore, when nitrates enter the human body, they can cause health problems such as methemoglobinemia (Dong et al. 2020). Although nitrogen fertilizer utilization in China has increased to approximately 40%, it still remains significantly lower than that in developed countries, namely 70% in Occident (Liu et al. 2022a). Achieving a rational and efficient use of nitrogen fertilizers in China is essential to ensure both crop yields and environmental sustainability, but it remains a major challenge.

In response to these issues, existing mitigation strategies have focused on reducing NO_3^-–N loss and enhancing NH_4^+–N retention (Chen et al. 2010; Liu et al. 2022b). NH_4^+–N, in contrast to NO_3^-–N, is less susceptible to leaching and is often more readily available for plant uptake in certain soil conditions (Cao et al. 2019). The immobilization of NH_4^+–N in the soil can thus serve as an effective strategy to minimize nitrate leaching, improving both NUE and environmental outcomes. Recent studies have suggested that the incorporation of materials such as biochar can help alleviate nitrate leaching while promoting NH_4^+–N immobilization in the soil, offering a potential solution to the challenges of nitrogen management in agriculture (Chandra et al. 2020; Zhang et al. 2023a; Wu et al. 2024a). The alkaline functional groups, non-traditional hydrogen bonds, and cations, such as K^+, Fe^{3+}, and Ca^{2+}, on the biochar surface can

adsorb and immobilize nitrate nitrogen via intermolecular forces and bridge formation (Jin et al. 2016). Additionally, oxygen-containing functional groups on the biochar surface give it a high density of negative charges, which can firmly adsorb ammonium ions, organic nitrogen and enzymes onto its surface under the influence of electrostatic forces (Cao et al. 2019; Hossain et al. 2020). Once immobilized via adsorption, it becomes difficult for these components to decompose or be catalyze, thereby reducing the leaching of nitrate nitrogen in the soil. Therefore, the use of biochar is important in controlling nutrient leaching and thus preventing environmental pollution.

Modified biochar exhibits significantly stronger nitrogen adsorption capacity compared to unmodified biochar. Chandra et al. (2020) reported that chemically modified biochar (Fe/Al/MgO) could realize a maximum NO_3^-–N adsorption capacity ranging from 62 mg g^{-1} to 95 mg g^{-1}, which indicates its considerable potential for application. Among the modified biochars, iron-modified biochar has emerged as a novel material with excellent magnetic properties and biological activity, making it highly promising for soil remediation and environmental pollution control (Liu et al. 2020b; Wan et al. 2020). It contains mineral phases such as magnetite, hematite, and zero-valent iron, which typically exist in nanoparticle form on the surface or within the pores of biochar (Chen et al. 2024). The physical and chemical characteristics of iron-modified biochar are highly variable and affected by factors like magnetic particle type and the impregnation method, which in turn affect its nitrogen pollutant adsorption mechanism and capacity (Su et al. 2023). Scanning electron microscopy (SEM) and transmission electron microscopy (TEM) analyses have also shown that surface morphology of iron-modified biochar is strongly dependent on precursor materials and synthesis methods (Yi et al. 2019). A majority of iron-modified biochars exhibit smooth surfaces and well-developed pore structures, with iron oxides chemically which are bonded to biochar matrix and always distributed within the pores or on the surface of the biochar (Dewage et al. 2018). Characterization techniques, such as X-ray diffraction (XRD) and X-ray photoelectron spectroscopy (XPS), have confirmed that the predominant iron phases in iron-modified biochar are α-Fe_2O_3, γ-Fe_2O_3, and other iron oxides (Cai et al. 2017).

Previous studies have shown that due to its strong reductive properties, large specific surface area, and cost-effectiveness, nanoscale zero-valent iron (nZVI) has been broadly applied for removing nitrate from wastewater (Afzal et al. 2024; Guo et al. 2023). However, nZVI has limitations due to several drawbacks such as its susceptibility to oxidation in air, magnetic interference, aggregation and instability (Xu et al. 2024b). Biochar with large pore volume and surface functional groups can serve as a support material for nZVI, and effectively alleviate its aggregation issues and enhancing its removal performance (Wang et al. 2019). While nZVI-loaded biochar is not a new modification approach, several studies have explored its use for improving various environmental processes (He et al. 2018; Li et al. 2024; Guo et al. 2023). However, most of these studies have not focused on optimizing the performance of nZVI@BC by adjusting the iron-to-carbon (Fe/C) ratio. This study builds on previous work that used K_2FeO_4 as a modifying agent in combination with biochar, which enhanced nZVI dispersion and surface reactivity (Ma et al. 2021). Unlike earlier studies, we aim to investigate the impact of varying the Fe/C ratio on nitrate reduction efficiency and nitrogen retention. Additionally, our study uniquely addresses the challenge of mitigating NO_3^-–N leaching, a concern that has not been fully addressed in previous research. Through this investigation, we hope to provide a more comprehensive understanding of the mechanisms underlying the enhanced performance of nZVI@BC composites, offering a promising strategy for remediating agricultural non-point source pollution and advancing sustainable nitrogen management.

2 Materials and methods

2.1 Preparation of biochar loaded with nano zero-valent iron

The collected corn stover was air-dried, surface soil was removed, and the material was rinsed three times with deionized water and dried at 105 °C for 8 h. Subsequently, the dried stover was ground using a pulverizer and sieved through a 20-mesh nylon screen. It was then pyrolyzed at 600 °C to prepare biochar, as previous studies have indicated that this temperature provides a balanced yield of biochar with a significant surface area and preserves critical functional groups essential for nutrient retention and pollutant sorption (Sun et al. 2014; Hu et al. 2017). Finally, the biochar was ground and passed through a 100-mesh nylon screen, thus obtaining the corn stover biochar (BC), and stored for further use. The detailed measurement methods are provided in the supplementary material.

The corn stover biochar (BC) prepared as described above was mixed with four different doses of potassium ferrate (K_2FeO_4) at mass ratios of 0.2, 0.4, 0.6, and 0.8 of iron to biochar. The mixture was then put in a zirconia jar (500 mL) in a planetary ball mill (YXQM-2L) with zirconia balls (diameter 5 mm, 565 g per jar, ball-to-material ratio 20:1). The operation was carried out in ambient air, with the ball mill set to a speed of 500 rpm, alternating between 15 min of forward rotation and 15 min of reverse rotation for a total of 30 min (Chen et al. 2024).

After milling, the mixed solids were gathered and transferred to a muffle furnace for secondary calcination. Nitrogen gas (N_2) was introduced into the furnace at 0.1 m^3 h^{-1} flow rate, and the temperature was increased at at a rate of 5 °C min^{-1} before reaching 800 °C (Sun et al. 2014; Hu et al. 2017), at which it was maintained for 2 h. Following natural cooling, the black solid was collected, rinsed multiple times with deionized water before drying in 70–80 °C oven. Finally, the solid was ground and passed through 100-mesh nylon screen and stored for further use, yielding the nano zero-valent iron-loaded biochar (nZVI@BC). Samples were labeled as nZVI@BC0.2, nZVI@BC0.4, nZVI@BC0.6, and nZVI@BC0.8, respectively.

2.2 Characterization

The elemental composition (C, H, O, and N) of the materials was measured using an elemental analyzer (Vario Micro Cube, Germany). The crystal structure of the materials was analyzed using X-ray diffraction (XRD, Bruker D8 Advance). Fourier-transform infrared spectroscopy (FTIR, Nicolet 6700) with wavenumber range of 400–4000 cm^{-1} was used to analyze the surface functional groups of the materials. 2D-COS synchronous and asynchronous spectra were used to investigate the chemical interactions and dynamic changes of the composite materials, with synchronous spectra revealing frequency interactions and asynchronous spectra highlighting property evolution (Kong et al. 2021). The design calculations for 2D-COS were carried out following the methodology outlined by Noda and Ozaki (2004). The analysis was conducted using 2D Shige software (Kwansei Gakuin University, Japan), with spectral data pretreated by Savitzky-Golay smoothing prior to 2D analysis (Zhang et al. 2023b). A surface area analyzer (BET, MicrotracBEL Corp.) was applied to measure the pore size distribution and specific surface area of the biochar. The morphology of the biochar and its surface elemental composition were analyzed using a transmission electron microscope (TEM) and energy dispersive spectroscopy (EDS) (JEOL JEM 2100F, Japan).The surface chemical properties of the materials were measured by X-ray photoelectron spectroscopy (XPS, AXIS Supra, Kratos Analytical Ltd). The physicochemical characteristics of pristine biochar and nZVI@BC have been given in Table S1. A schematic representation of the steps involved in the preparation of nZVI@BC is provided in Fig. 1.

2.3 Nitrate nitrogen removal efficiency of nZVI@BC

2.3.1 Removal of nitrogen species including nitrate nitrogen using nZVI@BC under different pH conditions

A total of 0.1 g of biochar (BC, nZVI@BC0.2, nZVI@BC0.4, nZVI@BC0.6, and nZVI@BC0.8) was weighed and added into 50 mL centrifuge tubes, and 40 mL of 100 mg L^{-1} KNO_3 solution was added to each tube. Solution pH was then

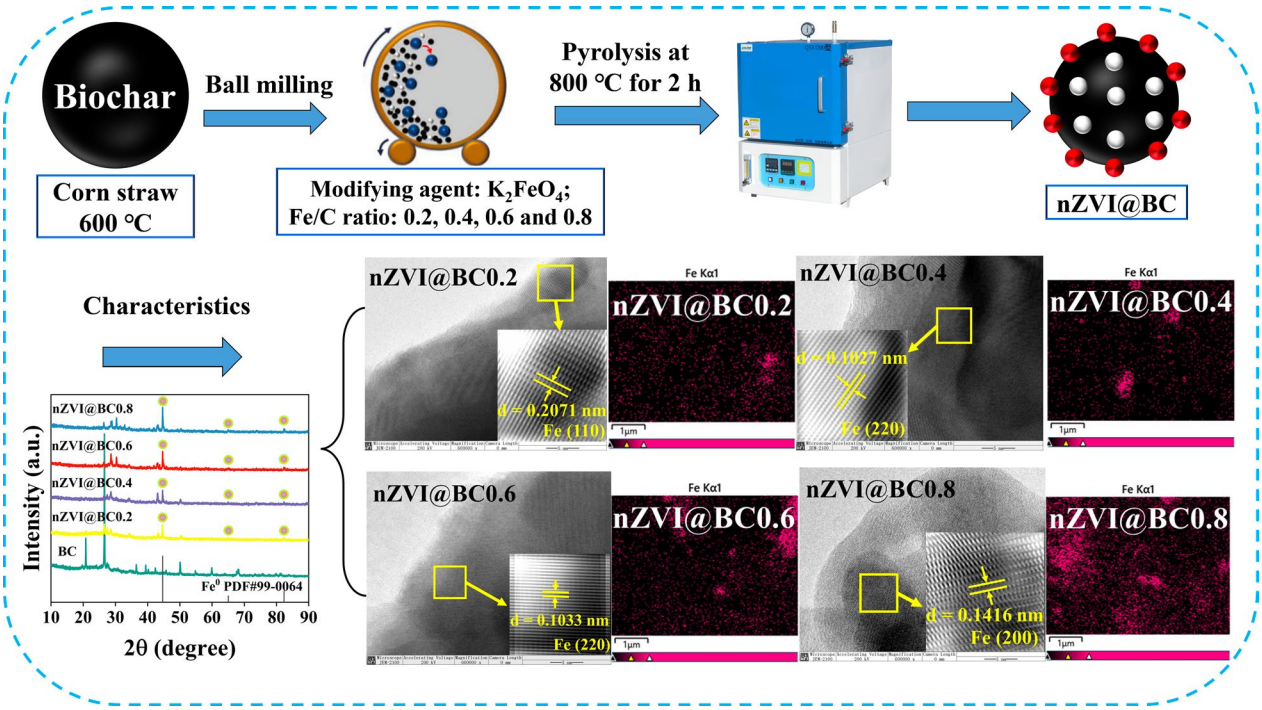

Fig. 1 Flowchart illustrating the preparation processes and characterization of nZVI@BC

regulated using 0.5 mol L^{-1} HCl/NaOH to achieve original 2, 3, 4, 5, 6, 7, 8, 9, 10, 11, and 12 pH values. The specimens were shaken at 25 °C constant temperature in a shaker, at 200 rpm for 24 h. Subsequently, the collected leachate samples were immediately filtered through 0.22 μm membranes, which effectively removed most bacteria, including mycoplasma (Kim et al. 2023). The resulting filtrate was then gathered in 15 mL centrifuge tubes, labeled accordingly, and stored at − 20 °C for further analysis. Nitrogen species, including nitrate (NO_3^-–N), ammonium (NH_4^+–N), and nitrite (NO_2^-–N), were quantified using an AA3 AutoAnalyzer (Bran+Luebbe, Germany). The nitrate removal efficiency ($R_{nitrate}$), nitrite selectivity ($S_{nitrite}$), ammonia selectivity ($S_{ammonia}$), and nitrogen gas selectivity ($S_{nitrogen}$) were calculated using the following formulae (He et al. 2018):

$$R_{nitrate}(\%) = \frac{[NO_3^-]_i - [NO_3^-]_f}{[NO_3^-]_i} \quad (2\text{-}1)$$

$$S_{nitrate}(\%) = \frac{[NO_2^-]_f}{[NO_3^-]_i - [NO_3^-]_f} \quad (2\text{-}2)$$

$$S_{ammonia}(\%) = \frac{[NH_4^+]_f}{[NO_3^-]_i - [NO_3^-]_f} \quad (2\text{-}3)$$

$$S_{nitrogen}(\%) = \frac{[NO_3^-]_i - [NO_3^-]_f - [NO_2^-]_f - [NO_4^+]_f}{[NO_3^-]_i - [NO_3^-]_f} \quad (2\text{-}4)$$

where $[NO_3^-]_i$ denotes initial concentrations of nitrate nitrogen (mg L^{-1}) whereas $[NO_3^-]_f$ represents final concentrations of nitrate nitrogen (mg L^{-1}), and $[NO_2^-]_f$ and $[NH_4^+]_f$ denote final concentrations of nitrite nitrogen and ammonium nitrogen (mg L^{-1}), respectively.

2.4 Adsorption of nitrate nitrogen by nZVI@BC

Adsorption kinetics experiment: 0.1 g of biochar was weighed totally and added into 50 mL centrifuge tubes, with 30 mL of 100 mg L^{-1} KNO_3 solution added to each tube. Such specimens were then subjected to shaking at 200 rpm for various time intervals (5, 10, 20, 30, 60, 90, 120, 180, 360, 720, and 1440 min) at 25 °C. 0.22 μm membrane filter was used to filter specimens, with resulting filtrate gathered in 15 mL centrifuge tubes, labeled accordingly, and stored at − 20 °C for further analysis. An AA3 AutoAnalyzer (Bran+Luebbe, Germany) was used to measure nitrate nitrogen (NO_3^-–N) concentrations in the filtrate. To analyze adsorption kinetics data, such results were fitted to the pseudo-first-order model, pseudo-second-order model, and intra-particle diffusion model (Elovich) (Ma et al. 2020). Kinetic model fitting used the equations as below:

$$\text{Pseudo} - \text{first} - \text{order} : Q_t = Q_e(1 - e^{-k_1 t}) \quad (2\text{-}5)$$

$$\text{Pseudo} - \text{second} - \text{order} : Q_t = \frac{k_2 Q_e^2 t}{1 + k_2 Q_e t} \quad (2\text{-}6)$$

$$\text{Elovich} : Q_t = a + b\ln t \quad (2\text{-}7)$$

in which Q_t (mg g^{-1}) and Q_e (mg g^{-1}) stand for amounts of nitrate nitrogen (NO_3^-–N) adsorbed at time t and at equilibrium, respectively; k_1 (h^{-1}) and k_2 (mg g^{-1} h^{-1}) are pseudo-first-order and pseudo-second-order rate constants, respectively; a and b refer to constants pertaining to adsorption capacity.

Adsorption isotherm experiment: 0.1 g of biochar was weighed totally and added into 50 mL centrifuge tubes, with 50 mL of KNO_3 solution at varying concentrations (20, 40, 60, 80, 100, 200, 400, 600, 800, and 1000 mg L^{-1}) added to each tube. Specimens were shaken at room temperature for 24 h. Subsequently, 0.22 μm membrane filter was utilized to filter specimens, with filtrate gathered in 15 mL centrifuge tubes, labeled accordingly, and stored at − 20 °C for further analysis. An AA3 AutoAnalyzer (Bran+Luebbe, Germany) was used to measure nitrate nitrogen (NO_3^-–N) concentrations in filtrate. To analyze adsorption isotherm data, such results were fitted to Langmuir, Freundlich, and Sips (Freundlich-Langmuir) models (Tran et al. 2021). Thermodynamic model fitting used the equations as below:

$$\text{Langmuir equation} : Q_e = \frac{Q_m K_L C_e}{1 + K_L C_e} \quad (2\text{-}8)$$

$$\text{Freundlich equation:} \ Q_e = K_F C_e^{1/n} \quad (2\text{-}9)$$

$$\text{Sips (Freundlich} - \text{Langmuir) equation} : Q_e = K_F C_e^{1/n} \quad (2\text{-}10)$$

where C_e (mg L^{-1}) represents the equilibrium concentration of NO_3^-–N, Q_e (mg g^{-1}) is the equilibrium adsorption capacity of NO_3^-–N; Q_m (mg g^{-1}) indicates the material's maximum adsorption capacity; K_L, K_F, K_{LF}, n, n_{LF}, and a_{LF} are the constants of the three models mentioned above.

2.5 Migration of nitrate and inhibition of leaching by nZVI@BC

2.5.1 Column migration experiment

The migration experiments were conducted in acrylic columns (height: 20.0 cm, diameter: 3.0 cm), which were filled with quartz sand. The packing material adopted was quartz sand with a 2 mm particle size. The

sand was first rinsed with ultrapure water to remove impurities, and soaked in 0.1 mol L^{-1} NaOH and HCl solutions for 24 h each to remove adsorbed metal ions and colloidal substances. Afterward, the quartz sand was rinsed again with ultrapure water and dried in the oven to remove moisture, resulting in purified quartz sand. The porosity of the packed column material was 0.31, and the pore volume (PV) was 43.7 mL.

A schematic representation of column setup is depicted in Fig. S1. nZVI@BC with different iron-to-carbon ratios (0.2, 0.4, 0.6, and 0.8) was mixed uniformly with the pure quartz sand obtained above at a 1% (w/w) addition rate, and then packed into the columns. Each treatment was performed in triplicate. The local irrigation rate (approximately 20 mL min^{-1}) was simulated using a peristaltic pump to mimic irrigation conditions. This irrigation rate was carefully selected based on typical local agricultural practices and the specific soil and crop conditions in the region (Yuan et al. 2023).

Effluent from the quartz sand columns was collected every 0.25 PV. The absorbance of the solutions from each treatment was measured using a UV–Vis spectrophotometer (UV-2700, Shimadzu Corporation, Japan) at wavelengths of 192 nm, 198 nm, 209 nm, 227 nm, and 248 nm (Fig. S2) to determine the concentration of biochar in the effluent and construct breakthrough curves. A standard absorbance curve for the biochar suspension was constructed using serial dilution, with correlation coefficients (R^2) of 0.9975, 0.9965, 0.9973, 0.9991, and 0.9974, respectively (Fig. S3).

Following column migration experiment and effluent from sand columns was collected, the quartz sand in the column was divided into 10 equal sections based on column height. Every 2 cm of quartz sand was sequentially removed and put into a 50 mL centrifuge tube. Then, 20 mL of deionized water was added, and the mixture was shaken for 2 h to release the biochar retained on the quartz sand particles. The biochar concentration was measured to determine its vertical distribution in the column, and a spatial retention curve was constructed.

2.5.2 Soil column leaching experiment

In this experiment, PVC cylindrical columns with caps at both the top and bottom were used to simulate soil leaching columns. Soil specimens adopted in our experiment were gathered from greenhouse vegetable field located in Wuqing District, Tianjin, China (39°32' N, 117°3' E). The field is mainly planted with cucumber/tomato or tomato/leafy vegetable rotation. Soil physicochemical properties are illustrated in Table S2. The soil was packed into the columns at approximately 1 g cm^{-3} fixed bulk density. Before the leaching started, deionized water was added to saturate the soil, and after equilibrating for 3 h, the columns were put in an incubator at 25 °C constant temperature. Leaching was simulated using a peristaltic pump to maintain a local irrigation rate of approximately 20 mL min^{-1}. Leachate specimens were collected on days 7, 14, 21, 28, and 35 of incubation, based on previous studies indicating significant cumulative nitrate leaching at weekly intervals (Wang et al. 2015; Bae et al. 2019). No samples were collected during the first 7 days to minimize transient variability and ensure steady-state conditions (Wang et al. 2015). Treatments included: blank control (CK), pristine biochar (BC), and nZVI@BC with different iron-to-carbon ratios (0.2, 0.4, 0.6, and 0.8), with a 1% addition rate for each. The concentrations of NO_3^- and NH_4^+ in the leachate were measured, and the cumulative distribution (retention) of NO_3^- and NH_4^+ in different soil layers (0–5 cm, 5–10 cm, 10–15 cm, and 15–20 cm) was measured.

2.6 Statistical analysis

The experimental data were organized utilizing Excel 2021. Statistical analysis was performed using the "stats" package in R 4.4.1. One-way analysis of variance (ANOVA) was performed to assess significant differences in ammonium nitrogen and nitrate nitrogen concentrations among treatments. Post hoc comparisons were conducted using both the least significant difference (LSD) test and Duncan's multiple range test at a significance level of $P < 0.05$. Pearson correlation coefficient was used to analyze linear correlation among variables. We performed structural equation modeling (SEM) using the "piecewiseSEM" package in R 4.4.1 to investigate direct and indirect influences of Fe/C ratio of biochar, physicochemical properties, structural and functional characteristics, and adsorption capacity on nitrate nitrogen removal efficiency, ensuring that the number of data points for each manifest variable was consistent and comparable across all variables. All images were plotted using Origin 2021 (OriginLab Corporation, Northampton, MA, USA).

3 Results and discussion

3.1 Potential of nZVI@BC at nitrate nitrogen reduction under different pH conditions

The treatments with nZVI@BC at varying pH showed a significant reduction in nitrate concentrations whereas pristine biochar showed a similar reduction in NO_3^-–N concentrations (Fig. 2a). This was also evident in the NH_4^+–N and NO_2^-–N concentrations (Fig. 2b, c). nZVI@BC effectively reduced nitrate to nitrite and ammonium nitrogen effectively. The highest ammonium nitrogen concentrations were observed at pH 2, reaching 22.01 mg L^{-1}, 24.94 mg L^{-1}, 41.68 mg L^{-1}, and 43.98 mg L^{-1} for nZVI@BC0.2, nZVI@BC0.4, nZVI@BC0.6, and nZVI@BC0.8, respectively (Fig. 2b). Similarly, at pH 2, the remaining

nitrate concentrations for nZVI@BC0.2, nZVI@BC0.4, nZVI@BC0.6, and nZVI@BC0.8 were 16.83 mg L^{-1}, 12.63 mg L^{-1}, 4.35 mg L^{-1}, and 2.85 mg L^{-1}, respectively, significantly less than those of BC treatment (Fig. 2a). The enhanced reduction capacity under acidic conditions can be attributed to the stronger reduction ability of nZVI in acidic environments. This suggests that the presence of nZVI dramatically enhances nitrate's reduction to ammonium nitrogen, especially under acidic conditions, where nZVI is more reactive and efficiently facilitates nitrate conversion. Lower pH reduced its oxidation and promoted the stability of nZVI, which in turn accelerates nitrate's conversion to ammonium nitrogen (Tang et al. 2021). Moreover, the increased surface reactivity of nZVI under acidic conditions further promoted the reduction reaction (Yuan et al. 2022). However, when the pH increased, the reduction capacity of nZVI@BC0.2 and nZVI@BC0.4 gradually decreased, whereas nZVI@BC0.6 and nZVI@BC0.8 maintained relatively stable reduction performance at pH values above 7. The decline in reduction efficiency with increasing pH, particularly for nZVI@BC0.2 and nZVI@BC0.4, is likely due to the increased oxidation of nZVI under neutral and alkaline conditions, leading to the formation of iron hydroxides (such as $Fe(OH)_3$), which reduce catalytic activity and inhibit nitrate reduction (Liu and Wang 2019). Nevertheless, higher nZVI loading in nZVI@BC0.6 and nZVI@BC0.8 improves nZVI dispersion and stability, mitigates oxidation effects, and maintains more stable reduction performance under alkaline conditions (Liu et al. 2024). Additionally, the concentration of nitrite nitrogen showed a downward trend as pH for all nZVI@BC treatments increases (Fig. 2c). The highest nitrite nitrogen concentrations at pH 2 were 16.66 mg L^{-1}, 16.90 mg L^{-1}, 12.76 mg L^{-1}, and 12.41 mg L^{-1} for nZVI@BC0.2, nZVI@BC0.4, nZVI@BC0.6, and nZVI@BC0.8, respectively. The decrease in NO_2^-–N concentration with increasing pH suggests that nitrite, an intermediate product of nitrate reduction, is further reduced to NH_4^+–N more efficiently under acidic conditions. This highlights the efficiency of nitrate reduction at low pH. Conversely, at higher pH, the nitrate reduction process slows, leading to the accumulation of higher nitrite concentrations. These findings underscore the significant impact of pH on both the efficiency and pathway of nitrate reduction by nZVI@BC. Furthermore, these interpretations were corroborated with the observation that the nitrate removal efficiency of all nZVI@BC treatments was dramatically higher than that of control (BC) across the entire pH range (Fig. 2d). The highest nitrate removal rate occurred at pH 2, and the values are 83.17%, 87.37%, 95.65%, and 97.16% for nZVI@BC0.2, nZVI@BC0.4, nZVI@BC0.6, and nZVI@BC0.8, respectively. The low pH conditions likely promote electron transfer and reduction of nitrate (Wei et al. 2018). As the pH increased, the nitrate removal efficiency gradually decreased, which indicates that the reduction process is less efficient under alkaline conditions. This decrease can be attributed to the oxidation of nZVI at higher pH as it reduces its catalytic efficiency and limits the reduction of nitrate (Guo et al. 2015).

Additionally, it can be surmised that an increased iron-to-carbon ratio at the same pH leads to higher selectivity for NH_4^+–N in the reduction products (Fig. 2e–h). This suggests that higher nZVI loading and iron content improve the nitrate reduction process by providing more active sites for electron transfer, which favors the production of NH_4^+ (Liu et al. 2022b). On the other hand, at the same iron-to-carbon ratio, the selectivity for N_2 increased by rising pH, indicating that the reduction pathway shifts toward nitrogen gas formation under more alkaline conditions (Tang et al. 2019). This shift is consistent with the known tendency of nZVI to reduce nitrate to nitrogen gas in more neutral to alkaline environments, where the formation of iron oxides is promoted, further altering the reduction pathway (Zhao et al. 2022).

The primary reaction pathways may involve several steps in the nitrate reduction process. At low pH, nitrate is first reduced to nitrite, as shown in reaction (1), and the resulting nitrite is further reduced to ammonium nitrogen, as indicated in reaction (2). These reactions are favored under acidic conditions as the increased availability of protons accelerates the reduction process (He et al. 2018).

$$Fe^0 + NO_3^- + 2H^+ \rightarrow Fe^{2+} + NO_2^- + H_2O \quad (1)$$

$$Fe^0 + NO_2^- + 8H^+ \rightarrow Fe^{2+} + NH_4^+ + 2H_2O \quad (2)$$

At higher pH, Fe_3O_4, Fe_2O_3 and other iron oxides are formed, the reactivity of nZVI may be reduced, and the

(See figure on next page.)

Fig. 2 Impact of disparate Fe/C ratios of nZVI@BC on nitrate removal at various pH values. **a** NO_3^-–N concentration; **b** NH_4^+–N concentration; **c** NO_2^-–N concentration; **d** the removal efficiency of nitrate nitrogen (R_{NO3}^-). Different lowercase letters indicate significant differences ($P < 0.05$) among treatments at the same pH level, as determined by one-way ANOVA followed by Duncan's multiple range test. Note: the insets illustrate concentrations of NH_4^+–N and NO_2^-–N treated by BC. Selectivity of nitrogen species by nZVI@BC with disparate Fe/C ratios at different pH values (**e**, **f**, **g** and **h**)

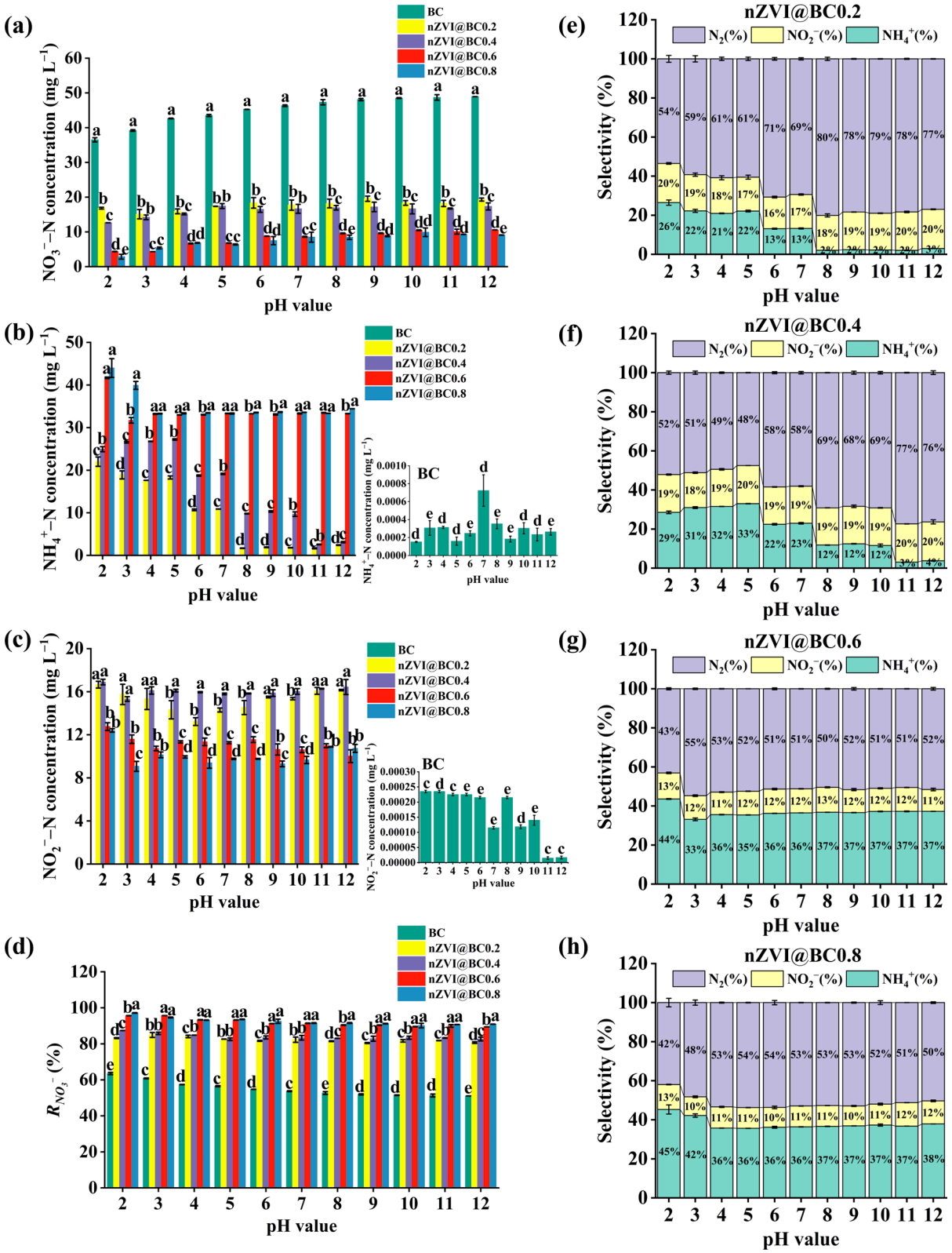

Fig. 2 (See legend on previous page.)

reduction process shifts to nitrogen gas formation, just as shown in reactions (3) and (4) (Liu and Wang 2019; Mokete et al. 2020).

$$10Fe^0 + 6NO_3^- + H_2O \xrightarrow{\text{Biochar}} 5Fe_2O_3 + 3N_2 \uparrow + 6OH^- \quad (3)$$

$$18Fe^0 + 10NO_3^- + 3Fe^{2+} + 2H_2O \xrightarrow{\text{Biochar}} 7Fe_3O_4 + 5N_2 \uparrow + 4OH^- \quad (4)$$

These results suggest that nitrate is more likely to be reduced to ammonium nitrogen under acidic conditions, whereas it might form nitrogen gas instead at high pH values. This pH-dependent shift in the reduction products is consistent with the observed trends in nitrate removal efficiency and the selectivity for different nitrogen species.

3.2 Effects of nZVI@BC on the adsorption of nitrate nitrogen

3.2.1 Adsorption kinetics

Founded upon above experimental outcomes, it was found that $R_{NO_3^-}$ tended to stabilize when the pH exceeded 7 (Fig. 2d). Additionally, since the pH of the selected test soil is around 7, batch adsorption tests were performed under neutral conditions.

Removing NO_3^-–N by nZVI@BC was significantly influenced by contact time (Fig. S4a–c). Compared to BC, all nZVI@BC treatments demonstrated higher removal efficiency, indicating that the ratio of iron to biochar and the contact time play a crucial role in NO_3^-–N removal. As the nZVI ratio increased, the removal efficiency of NO_3^-–N also improved, which may be attributed to the enhanced reduction of NO_3^-–N by nZVI (Xu et al. 2024a). The adsorption process followed two distinct stages: a rapid initial phase within the first hour, then a slower phase reaching (Fig. S4a–c). This suggests that adsorption process is initially dominated by surface adsorption, while the later stages may be controlled by internal diffusion or chemical reactions of NO_3^-–N, such as redox reactions with reduced metals like Fe^0 and Fe^{2+} (e.g., NO_3^- reduced to NH_4^+ or NO_2^-), or catalytic reactions on adsorption surface sites that facilitate the decomposition or transformation of NO_3^-–N into intermediate nitrogen species (Hei et al. 2022). Upon reaching adsorption equilibrium, the adsorption capacities (Q_e) for NO_3^-–N were 23.91 mg g^{-1}, 34.75 mg g^{-1}, 35.75 mg g^{-1}, 37.81 mg g^{-1}, and 38.77 mg g^{-1} for BC, nZVI@BC0.2, nZVI@BC0.4, nZVI@BC0.6, and nZVI@BC0.8, respectively. This indicates a gradual increase in removal capacity with higher nZVI ratios, likely due to the additional reduction sites provided by nZVI, which enhanced both adsorption and reduction processes (Yan et al. 2025).

Pseudo-first-order and pseudo-second-order models were utilized to analyze adsorption kinetics of NO_3^-–N. Pseudo-first-order kinetic model provided a better fit for the adsorption process of NO_3^-–N by BC ($R^2 = 0.945$) and nZVI@BC0.2 ($R^2 = 0.948$), which indicated a physical adsorption process (Table 1). This is likely attributed to the abundant porous structure and large surface area of biochar, which facilitate rapid adsorption through physical interactions, such as van der Waals forces or electrostatic attraction (Qiu et al. 2022; Tan et al. 2021). Good fit of pseudo-first-order model suggests that the adsorption process is initially rapid, with a substantial amount of adsorption occurring in a short period, followed by stabilization, indicating that physical adsorption dominates in the early stages and equilibrium is reached quickly. In contrast, pseudo-second-order model provided a better fit for nZVI@BC0.4 ($R^2 = 0.957$), nZVI@BC0.6 ($R^2 = 0.969$), and nZVI@BC0.8 ($R^2 = 0.998$), suggesting that these materials primarily undergo chemical adsorption. Introducing nZVI enhanced surface area and provided additional adsorption sites through surface chemical reactions or electron transfer mechanisms, thus promoting chemical adsorption (Awang et al. 2023; Wang et al. 2019). The better fit to pseudo-second-order model further supports the conclusion that the adsorption process is controlled by chemical reactions, with the adsorption rate slowed as the system approaches equilibrium.

3.2.2 Adsorption isotherms

The adsorption isotherm results indicated that nZVI@BC significantly increased the adsorption capacity (Q_e) of NO_3^-–N when the equilibrium concentration (C_e) rose,

Table 1 Kinetic model parameters for the adsorption of NO_3^-–N

Treatments	Pseudo-first-order			Pseudo-second-order			Elovich		
	Q_e (mg g^{-1})	k_1	R^2	Q_e (mg g^{-1})	k_2	R^2	a	b	R^2
BC	23.907	0.090	0.945	26.214	0.006	0.930	12,148.613	0.547	0.439
nZVI@BC0.2	34.175	0.174	0.948	34.554	0.015	0.843	1.748	0.907	0.449
nZVI@BC0.4	34.181	0.110	0.924	35.094	0.004	0.957	167.609	0.282	0.838
nZVI@BC0.6	35.083	0.133	0.935	35.755	0.007	0.969	14,345.009	0.425	0.938
nZVI@BC0.8	34.163	0.092	0.978	36.253	0.003	0.998	13.631	0.195	0.950

and compared to BC, it demonstrated an improved Q_e (Fig. S4d–f). The increase can be attributed to enhanced surface activity and adsorption sites on biochar after nZVI addition, as well as nZVI's inherent strong adsorption and reduction abilities (Awang et al. 2023; Wang et al. 2019). nZVI also releases iron ions that alter the surface charge of biochar, thereby boosting NO_3^-–N adsorption (Xu et al. 2024a). Previous studies have shown that nZVI provides more adsorption sites and enhances adsorption through reduction reactions, thereby increasing the overall Q_e (Liu and Wang 2019; Tang et al. 2021). At equilibrium, the maximum adsorption capacities (Q_m) for NO_3^-–N were 45.63 mg g^{-1}, 59.740 mg g^{-1}, 63.65 mg g^{-1}, 71.05 mg g^{-1}, and 84.55 mg g^{-1} for BC, nZVI@BC0.2, nZVI@BC0.4, nZVI@BC0.6, and nZVI@BC0.8, respectively, showing an obvious increase with higher nZVI ratio. This further confirms that nZVI is crucial to improving the adsorption efficiency of biochar.

The Sips model (Freundlich-Langmuir) best described the adsorption process ($R^2 = 0.965–0.998$), indicating a combination of monolayer and mixed adsorption mechanisms (Table 2). This suggests that NO_3^-–N adsorption involves surface chemical reactions and physical adsorption (Heydari et al. 2024; Liu et al. 2020a). As nZVI content increased, the adsorption capacity improved significantly, confirming that nZVI markedly enhanced the ability of biochar to adsorb NO_3^-–N. It could be ascribed to high reactivity and large surface area of nZVI , which creates additional adsorption sites and boosts capacity (He et al. 2018; Hei et al. 2022). The higher a_{LF} values in the Sips model further support this conclusion (Table 2), indicating that as nZVI proportion rises, both the driving force and adsorption capacity of the process are enhanced.

3.2.3 Adsorption mechanism of nitrate nitrogen by nZVI@BC

The XRD analysis revealed significant interactions between iron and nitrate in biochar. All nZVI@BC treatments (except BC) showed characteristic diffraction peaks of Fe^0 (PDF#99-0064) at $2\theta = 44.66°$, 65.22°, and 82.54°, with peak intensity increasing as the iron-to-biochar ratio rose, indicating higher Fe^0 content. (Fig. 3a). This suggests that as the iron-to-biochar ratio increases, the reduction of iron is enhanced, leading to a higher Fe^0 content, which in turn strengthens the characteristic diffraction peaks in the XRD spectra (Gillingham et al. 2022). After nitrate adsorption, the XRD spectra showed additional peaks corresponding to Fe_2O_3, FeO, and the complex $((NO)_3(NO_3))(Fe(NO_3)_4)_2$, confirming the interaction between iron and nitrate ions (Fig. 3g). Particularly, the complex $((NO)_3(NO_3))(Fe(NO_3)_4)_2$ peak indicates that iron forms a specific complex with nitrate ions, further confirming the successful adsorption of nitrate (Perveen et al. 2021). The presence of nZVI in biochar enhances nitrate adsorption, stability, and immobilization through complexation, improving its efficiency in removing nitrate nitrogen. (Zhang et al. 2020, 2023a).

XPS analysis exhibited immense changes in chemical states of iron in BC and nZVI@BC before (Fig. 4b–f) and after (Fig.3h–l) nitrate adsorption. This observation aligns with Wang et al. (2019), who found that Fe^{3+} made up 72% of the total iron in biochar without nZVI, suggesting that iron predominantly exists in the oxidized form during preparation, limiting its electron-donating capacity in denitrification. In this study, Fe^{3+} made up 71.38% of the total iron in pristine biochar, with Fe^{2+} at 28.62%, confirming the limited reduction potential of biochar alone. After introducing nZVI, Fe^{2+} in nZVI@BC0.2 increased to 39.59%, while Fe^{3+} decreased to 60.41%, indicating that nZVI promoted the partial reduction of Fe^{3+} to Fe^{2+}, enhancing the electron transfer capacity of the composite. This result aligns with Liu et al. (2021), who reported a 12% increase in Fe^{2+} and a 68% nitrate removal efficiency in biochar loaded with 10% nZVI. As nZVI loading increased to nZVI@BC0.4, Fe^{2+} rose to 55.96% and Fe^{3+} dropped to 35.34%, accompanied by a decrease in satellite peak intensity, indicating continued Fe^{3+} reduction and inhibition of oxidation. The highest Fe^{2+} content of 70.8% was observed in nZVI@BC0.6, indicating that this nZVI loading maximized the reduction state of iron. This is consistent with Chen et al. (2010), who reported 72.5% Fe^{2+} at 60% nZVI loading, reflecting enhanced redox potential and electron transfer capacity. Increasing the nZVI loading to nZVI@BC0.8 caused

Table 2 Isotherm model parameters for the adsorption of NO_3^-–N

Treatments	Langmuir			Freundlich			Sips (Freundlich-Langmuir)			
	Q_m (mg g^{-1})	K_L	R^2	K_F	n	R^2	K_{LF}	a_{LF}	n_{LF}	R^2
BC	46.467	0.015	0.926	6.459	0.297	0.831	2.142	44.397	91.408	0.965
nZVI@BC0.2	66.088	0.011	0.926	6.040	0.355	0.796	1.813	60.477	93.648	0.972
nZVI@BC0.4	63.910	0.001	0.998	5.602	0.381	0.823	1.664	67.088	94.807	0.995
nZVI@BC0.6	83.763	0.007	0.992	3.580	0.444	0.944	0.024	78.284	2.195	0.998
nZVI@BC0.8	86.874	0.003	0.997	1.956	0.586	0.922	0.013	93.114	1.558	0.997

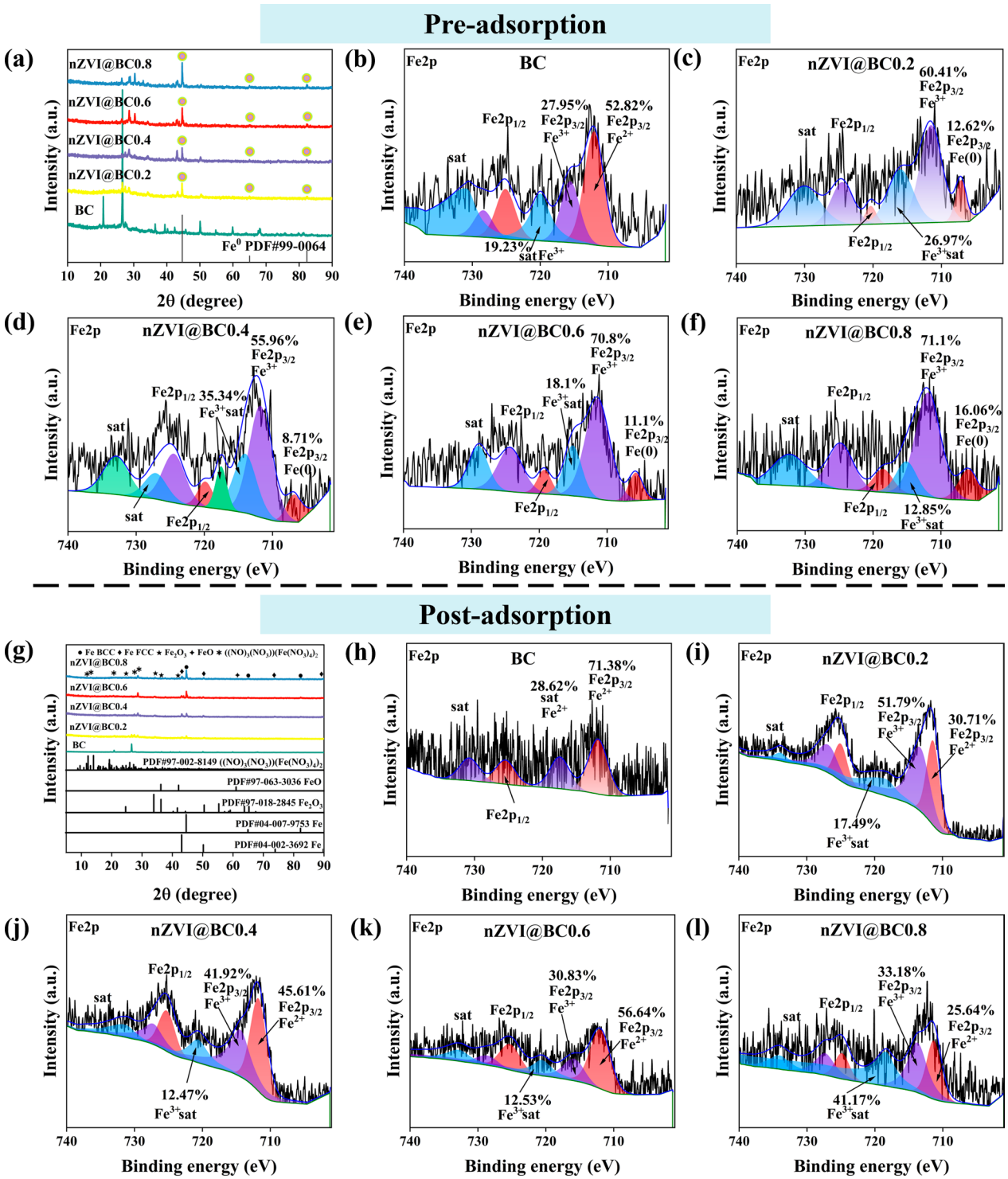

Fig. 3 XRD patterns (**a**) and XPS spectra (**b**, **c**, **d**, **e** and **f**) of pristine biochar and nZVI@BC before nitrate nitrogen adsorption. XRD patterns (**g**) and XPS spectra (**h**, **i**, **j**, **k** and **l**) of pristine biochar and nZVI@BC after nitrate nitrogen adsorption

Fe^{2+} to drop sharply to 16.06%, while Fe^{3+} rose to 71.1%, with enhanced satellite peaks, indicating that excess nZVI induced Fe^{2+} reoxidation and surface accumulation of oxidized iron, impairing nitrate removal. After nitrate adsorption, Fe^{2+} decreased and Fe^{3+} increased in all specimens (Fig. 3h–l), indicating Fe^{2+} oxidation to Fe^{3+}, and

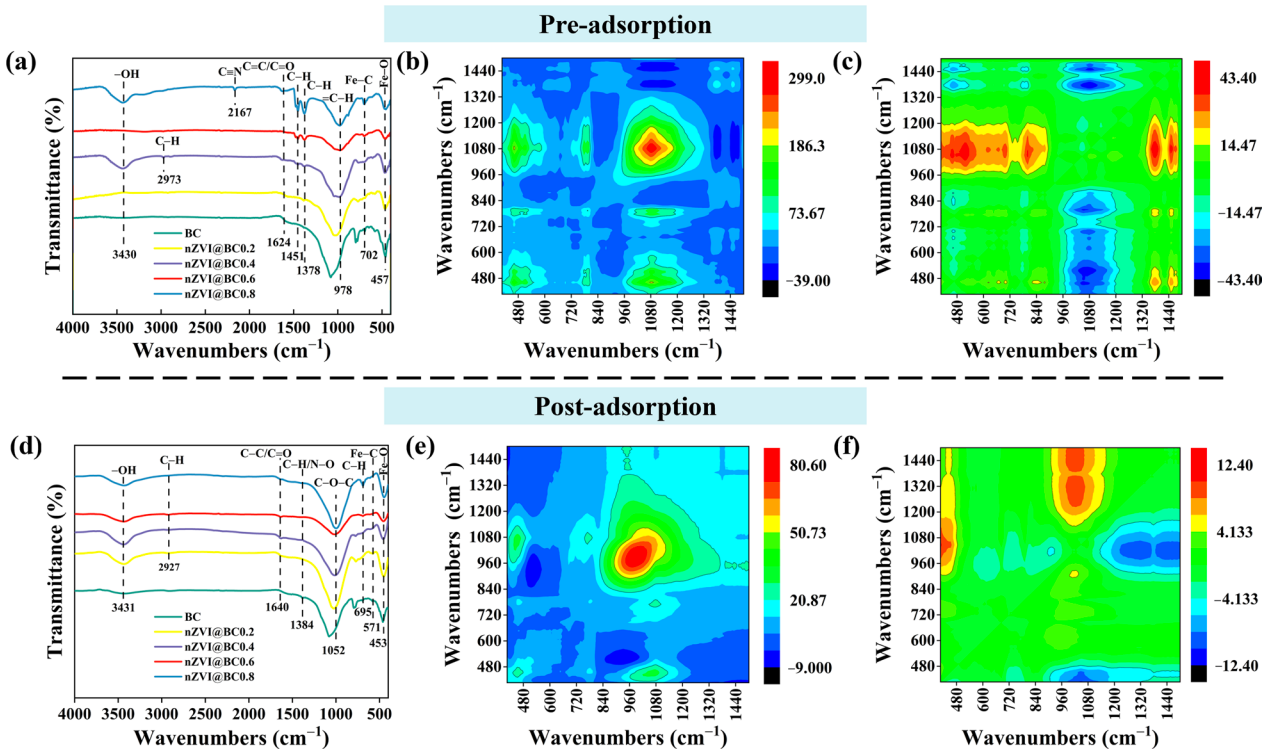

Fig. 4 FTIR spectra (**a**), 2D-COS synchronous spectra (**b**) and asynchronous spectra (**c**) of pristine biochar and nZVI@BC before nitrate adsorption. FTIR spectra (**d**), 2D-COS synchronous spectra (**e**) and asynchronous spectra (**f**) of pristine biochar and nZVI@BC after nitrate adsorption

highlighting iron's role as an electron donor and redox mediator in nitrate removal. (Huang et al. 2021; Fan et al. 2025). In pristine biochar, Fe^{2+} increased slightly to 27.95% after adsorption, with Fe^{3+} at 52.82%, showing limited nitrate reduction. In contrast, nZVI@BC0.4 and nZVI@BC0.6 retained Fe^{2+} at 45.61% and 56.64%, respectively, demonstrating that moderate nZVI loading prevents iron oxidation, maintains high redox potential, and improves nitrate removal. These results align with Cao et al. (2019), who found that 40–60% nZVI loading preserved over 50% Fe^{2+} content after nitrate adsorption, supporting sustained denitrification. Conversely, in nZVI@BC0.8, Fe^{2+} dropped to 25.64% and satellite peaks increased to 41.17%, confirming that excess nZVI promotes surface oxidation, limiting nitrate removal. These results emphasize that moderate nZVI loading optimizes nitrate removal by enhancing the reduction potential, while excessive nZVI promotes oxidative side reactions, diminishing efficiency. Fine-tuning the iron-to-carbon ratio is therefore critical for optimizing the denitrification efficiency of nZVI-biochar composites.

The FTIR analysis (Fig. 4a) revealed that functional groups on biochar before adsorption included a broad peak at 3430 cm^{-1} corresponding to the stretching vibration of hydroxyl groups (–OH), a peak at 2973 cm^{-1} assigned to the stretching vibration of C–H bonds in alkanes, a peak at 2167 cm^{-1} attributed to the stretching vibration of C≡N bonds, and a peak at 1624 cm^{-1} associated with the stretching vibration of C=C or C=O. Moreover, peaks between 1000 cm^{-1} and 500 cm^{-1} indicated metal–organic interactions, such as C–Fe or Fe–O bonds. These functional groups provided active sites for interactions including hydrogen bonding, van der Waals forces, and π-π interactions during the adsorption process (Tan et al. 2021). The hydroxyl (–OH) groups, in particular, could form hydrogen bonds with water molecules or nitrate ions, which enhanced the adsorption of water-soluble contaminants (Sonal and Mishra 2021). The C–H stretching vibrations suggested a considerable presence of alkyl groups, which aided in adsorbing nonpolar or small molecules (Amin et al. 2016). After adsorption (Fig. 4d), significant changes in the functional group peaks were found, including appearance of C–O–C and Fe–C bonds, which indicated that introducing nZVI altered biochar's surface structure. Incorporating nZVI led to metalization of the biochar surface, especially formation of C–O–C and Fe–C bonds. The Fe–C bonds signified interaction between nZVI and biochar, which strengthened nitrate's adsorption (Zhang et al. 2023a).

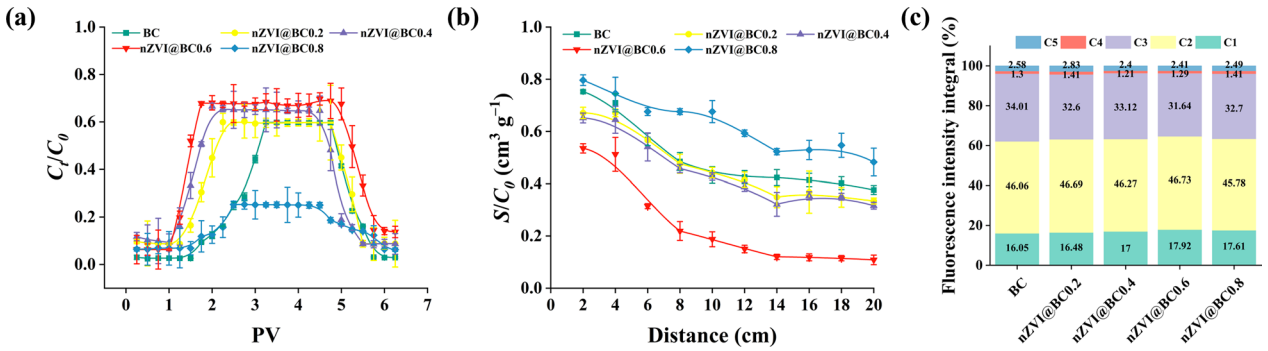

Fig. 5 Breakthrough curves (**a**), spatial retention curves (**b**), and 3D fluorescence components (**c**) of pristine biochar and nZVI@BC in the presence of nitrate nitrogen

In parallel, surface functional groups on biochar played a crucial role in stabilizing Fe^{2+} through coordination interactions. The C–O and C=O groups likely acted as electron-donating ligands that chelated Fe^{2+}, mitigating its rapid oxidation and facilitating continuous electron transfer to nitrate ions (Kong et al. 2021). The synchronous and asynchronous spectra further indicated early transformation of polar groups such as C=O and C–N, while less polar groups like C–H transformed later (Fig. 4c, f; Table S3, S4), implying a preferential role of oxygen-containing groups in initiating nitrate activation. The relative stability of Fe–O bonds across treatments suggests their role as anchoring sites for nitrate molecules, enhancing contact between the electron donor (Fe^{2+}) and the electron acceptor (NO_3^-) (Gao et al. 2022).

To sum up, the coordinated evolution of iron valence states and functional groups illustrates a synergistic mechanism, wherein moderate nZVI loading enhances the redox potential via sustained Fe^{2+} availability and its interaction with reactive surface sites on biochar. In contrast, excessive nZVI disrupts this balance by accelerating iron oxidation and inhibiting denitrification. Therefore, fine-tuning the Fe/C ratio is essential to optimize both the structural stability and functional performance of nZVI@BC composites in nitrate removal applications.

3.3 Influences of nZVI@BC upon migration and nitrate nitrogen leaching inhibition

3.3.1 Nitrate nitrogen impact on the migration behavior of nZVI@BC

Migration behavior of nZVI@BC is greatly influenced by nitrate nitrogen. The breakthrough curve (Fig. 5a) showed that nZVI@BC0.6 had the highest effluent ratio (0.68) in the presence of KNO_3 (50 mg L^{-1}), while nZVI@BC0.8 exhibited the lowest ratio (0.25), indicating a stronger migration capacity for nZVI@BC0.6. This was pertaining to biochar's physicochemical properties, particularly in its larger pore structure, surface hydrophilicity, and surface functional groups (Tan et al. 2021). nZVI@BC0.6 had a larger specific surface area and a more abundant microporous structure (Table S1), providing more adsorption sites for KNO_3, thereby increasing its migration ability by facilitating better contact between the biochar and KNO_3 molecules in the solution (Tu et al. 2021). The spatial retention curve (Fig. 5b) further revealed the spatial distribution characteristics of biochar within the packed column. Biochar exhibited significant retention within the 0–8 cm range at the column inlet, and as the column depth increased, the retention gradually decreased and stabilized. This phenomenon is closely related to biochar's adsorption properties and pore structure.

Three-dimensional fluorescence spectra analysis (Fig. S4) revealed that nZVI@BC0.6 contained a higher proportion of low molecular weight organic compounds (C1 and C2; 64.65%), which are highly hydrophilic (Fig. 6c). These organic substances improve dispersion and prevent biochar aggregation in water, enhancing its migration capacity. This finding aligns with Zhao et al. (2018), who reported that low molecular weight compounds enhance nanoparticle dispersion by increasing surface hydrophilicity. In contrast, nZVI@BC0.8 had a lower effluent ratio (0.25) due to its smaller surface area, denser pore structure, and lower proportion of low molecular weight organic compounds. These factors limit its dispersion and migration in aqueous solutions. The XPS C1s spectrum of biochar showed that the C–C/C=C ratio in nZVI@BC0.6 was highest at 67.81% (Fig. S5). This nonpolar structure reduces surface interactions with the surrounding environment (e.g., water and soil), enhancing particle mobility in the medium (Wang et al. 2019). It also minimizes aggregation of nZVI particles on the biochar surface, resulting in better dispersion and increased mobility of nZVI@BC0.6.

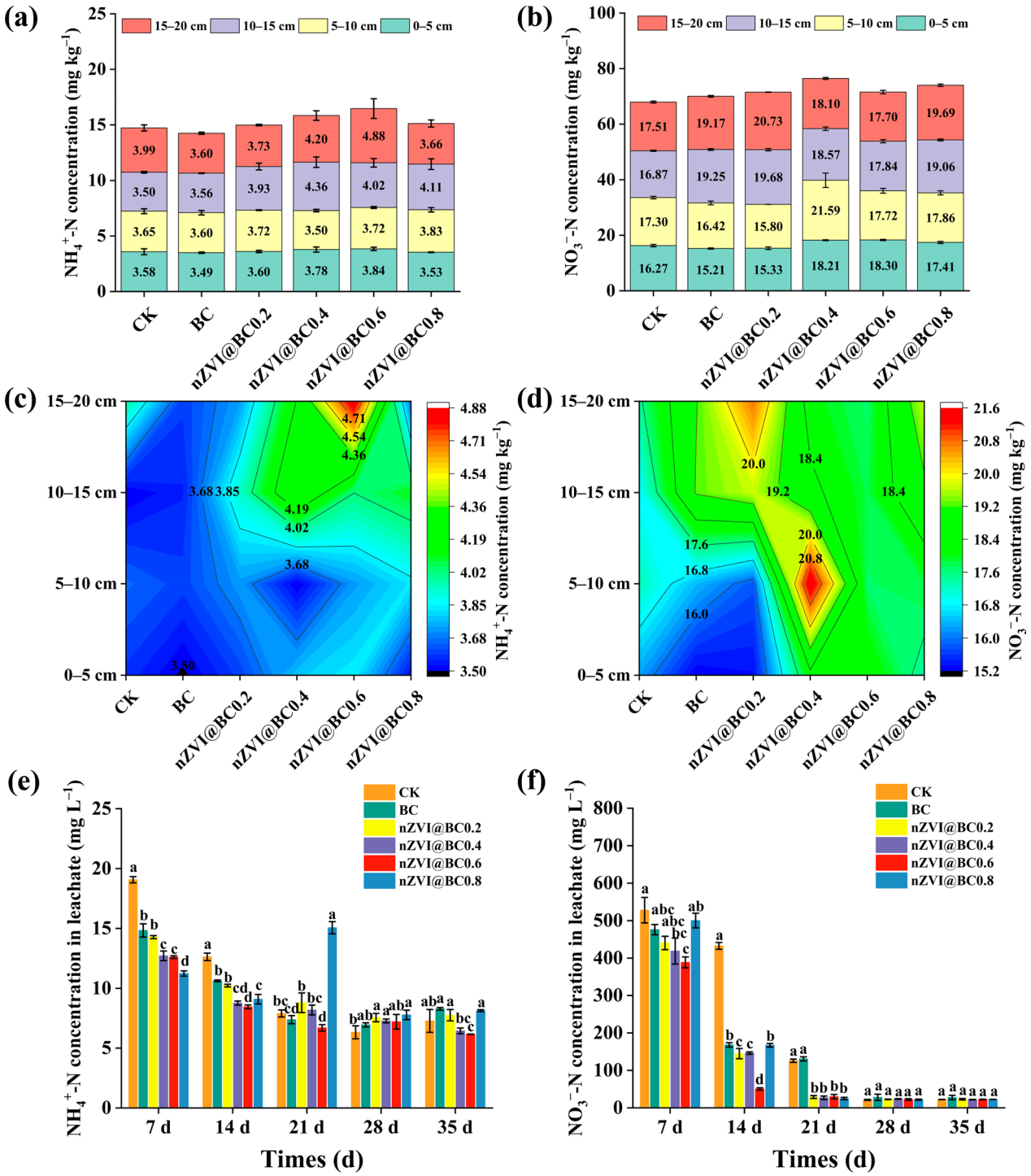

Fig. 6 Interception effect of nZVI@BC on soil nitrate nitrogen leaching Distribution characteristics of NH_4^+–N and NO_3^-–N in soil columns (**a**, **b**, **c** and **d**). NH_4^+–N and NO_3^--N concentrations in leachate from soil columns (**e** and **f**). Disparate lowercase letters stand for considerable disparity ($P < 0.05$) between treatments synchronously according to Duncan test

3.3.2 Contribution of nZVI@BC to nitrogen leaching in soil

The leaching column experiment demonstrated that nZVI@BC significantly increased the residual NH_4^+–N and NO_3^-–N in the soil column compared to the control and BC, with nZVI@BC0.6 showing the most remarkable effects (Fig. 6a–d). This can be primarily attributed

to the strong reducibility of nZVI, which inhibits the nitrification and reduces the oxidation rate of NH_4^+–N (Afzal et al. 2024). Meanwhile, porous structure and high specific surface area of biochar enhance nitrogen retention (Zhao et al. 2024). nZVI can lower soil Eh, suppressing nitrifying bacterial activity, while its surface activity enhances the adsorption of NH_4^+–N (Dissanayaka Mudiyanselage et al. 2020). Simultaneously, biochar weakly bonded with nitrogen via carboxyl and phenolic hydroxyl groups, enhancing nitrogen fixation efficiency. (Cao et al. 2019). In our work, NH_4^+–N content in nZVI@BC0.6 reached 17.22 mg kg^{-1}, 17.82% higher than CK, while NO_3^-–N reached 72.36 mg kg^{-1}, an 8.01% increase (Fig. 6a, b). Notably, in the 15–20 cm soil layer, the residual NH_4^+–N and NO_3^-–N contents were 4.88 mg kg^{-1} and 18.10 mg kg^{-1}, respectively, highlighting enhanced nitrogen retention (Fig. 6c, d). It has been previously reported that biochar can enhance nitrogen adsorption and fixation by improving cation exchange capacity (CEC) and altering the pore structure of deeper soils (Hossain et al. 2020). In summary, nZVI@BC0.6 exhibited remarkable advantages in reducing nitrogen leaching losses and enhancing soil nitrogen retention capacity.

The leaching experiment revealed that nZVI@BC treatments significantly mitigated nitrogen losses in the leachate, with the nZVI@BC0.6 treatment exhibiting the most notable performance due to its strong synergistic effects of adsorption and reduction of nitrate nitrogen (Fig. 6e, f). On day 7, NO_3^-–N concentration in the leachate of nZVI@BC0.6 was 26.44% lower than that of CK (390.56 mg L^{-1} vs. 530.92 mg L^{-1}), due to nZVI lowering the Eh, inhibiting nitrification, and biochar's adsorption of NO_3^-–N, thereby preventing its further loss into the leachate (Jin et al. 2016). By day 14, the NO_3^-–N concentration of nZVI@BC0.6 decreased by 71.31% compared to CK (78.85 mg L^{-1} vs. 274.81 mg L^{-1}), with nZVI facilitating abiotic denitrification through electron transfer and biochar enhancing soil cation exchange capacity (CEC), which stabilized nitrate retention (Rushimisha et al. 2024). Additionally, a temporary increase in NH_4^+–N on day 21 (21.45 mg L^{-1}) may have resulted from competitive ion exchange or desorption (Meng et al. 2022), but the concentration stabilized at 8.69 mg L^{-1} by day 28, indicating the system's self-regulating capacity, where re-adsorption and nZVI re-oxidation enhanced NH_4^+–N retention (Pei et al. 2024). While previous studies have demonstrated the individual effects of nZVI and biochar on nitrogen retention, our results show that the nZVI@BC composite, particularly nZVI@BC0.6, achieves superior performance by integrating reduction and adsorption mechanisms. Zhang et al. (2023a) showed that nZVI effectively reduced nitrate concentrations in contaminated water through its reductive capabilities, while Wang et al. (2019) demonstrated that biochar significantly improved nitrogen retention in soils by adsorbing ammonium and nitrate ions. In comparison, our study highlights the synergy between nZVI and biochar, showing that the combined nZVI@BC

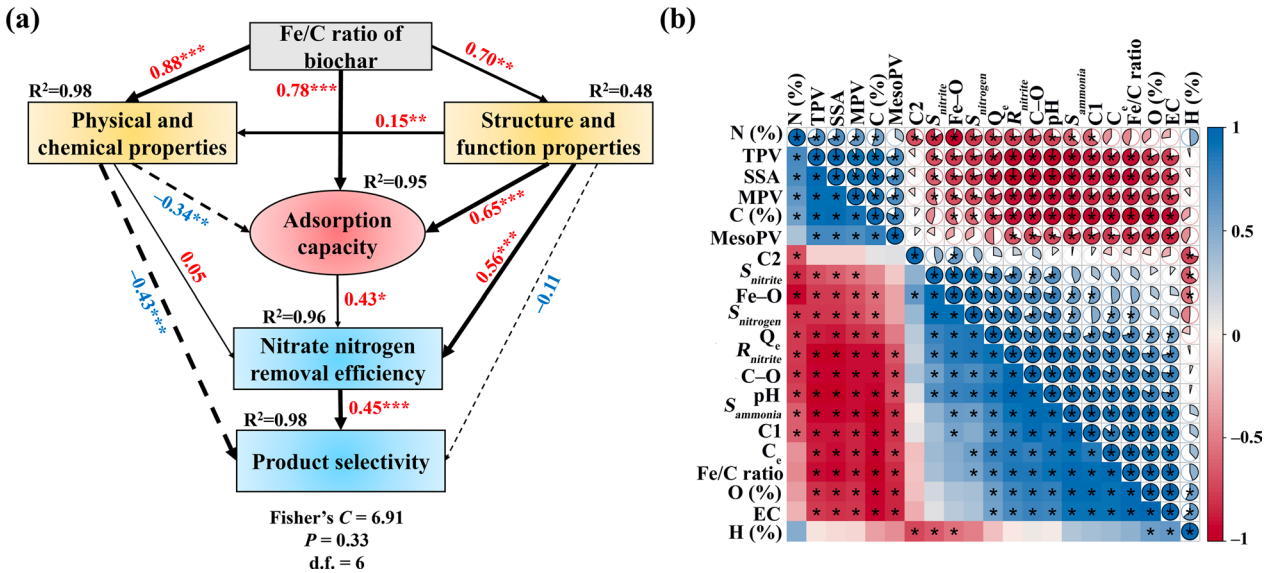

Fig. 7 SEM revealed direct and indirect influences of Fe/C ratio, physicochemical properties, structural–functional characteristics, and adsorption capacity of biochar upon nitrate nitrogen removal efficiency. **a** Pathway model. Positive and negative associations are indicated by solid and dotted lines, respectively. Numbers on the lines are path coefficients (λ). λ ranges from 0 to 1, the greater the coefficient, the stronger the relationship between the two variables. The R^2 represents proportion of variance explained. Levels of significance: $^*P < 0.05$, $^{**}P < 0.01$, and $^{***}P < 0.001$. **b** The correlation matrix showed the relationships between the indicators

composite has enhanced potential for mitigating nitrogen leaching in agricultural systems compared to these earlier approaches.

While these results demonstrate the effectiveness of nZVI@BC in reducing nitrogen leaching and enhancing nitrogen retention, the long-term stability and potential ecological risks in real complex soil environments require further investigation. Future research should focus on assessing the material's persistence, potential toxicity, and interactions with soil microorganisms to evaluate its long-term viability and environmental impact in large-scale applications.

3.4 SEM analysis of nitrate removal efficiency in nZVI@BC systems

The structural equation model (SEM) and correlation matrix analysis collectively revealed the influence of the Fe/C ratio of biochar, physicochemical properties, structural and functional characteristics, and adsorption capacity on nitrate nitrogen removal efficiency (Fig. 7a, b). The SEM results indicated that the Fe/C ratio significantly enhances adsorption capacity ($R^2 = 0.95$) by regulating physicochemical properties (path coefficient = 0.78, $P < 0.001$) and structural and functional characteristics (path coefficient = 0.65, $P < 0.001$) (Fig. 7a). This, in turn, improved nitrate nitrogen removal efficiency (path coefficient = 0.43, $P < 0.05$) and product selectivity (path coefficient = 0.45, $P < 0.001$). Among these factors, structural and functional characteristics were crucial to enhancing adsorption capacity and nitrate nitrogen removal efficiency.

The correlation matrix analysis further elucidated the effects of different functional groups within structural and functional characteristics on adsorption capacity and nitrate nitrogen removal efficiency (Fig. 8b). The structural indices Fe–O, C–O, C1, and C2 all exhibited significant positive correlations with adsorption capacity (Q_e) and nitrate nitrogen removal efficiency (R) ($P_{nitrate} < 0.05$). Specifically, Fe–O showed a strong positive correlation with both Q_e ($r > 0.67$) and $R_{nitrate}$ ($r > 0.67$). It indicated that the presence of iron oxides contributed to enhancing $R_{nitrate}$ of biochar. Similarly, the C–O bond content was positively correlated with Q_e ($r > 0.33$) and $R_{nitrate}$ ($r > 0.33$), suggesting that carbonyl or ester groups facilitated the electron transfer process (Wang et al. 2023). Furthermore, positive correlations between the contents of C1 and C2 with Q_e and $R_{nitrate}$ indicated that different types of carbon-based functional groups synergistically affected adsorption performance and surface catalytic activity, and thereby promoted nitrate nitrogen removal (Dong et al. 2020).

To sum up, Fe–O, C–O, C1, and C2 within the structural and functional characteristics is crucial to enhancing adsorption capacity and to improving nitrate nitrogen removal efficiency. Such findings further support the SEM analysis, and highlight the importance of structural and functional characteristics in optimizing nitrate nitrogen removal performance.

4 Conclusions and expected contributions

This study demonstrated that nZVI@BC composites effectively mitigate nitrogen leaching and enhance nitrogen retention, with nZVI@BC0.6 showing the highest nitrate removal and ammonium retention. The reduction of NO_3^-–N to NH_4^+–N under acidic conditions was driven by the synergistic effects of nZVI's reducibility and biochar's adsorption capacity, with structural characteristics such as Fe–O, C–O, C1, and C2 playing a key role in improving both adsorption and nitrate removal efficiency. nZVI@BC0.6 also exhibited significant nitrogen retention in deeper soil layers and maintained stability under neutral and alkaline conditions, emphasizing its potential for long-term application.

The use of K_2FeO_4 for modification and secondary calcination results in a relatively low production cost, making nZVI@BC composites a cost-effective solution for large-scale agricultural applications. Although scalability remains a consideration, the technology's affordability and high-performance position it as a promising strategy for mitigating nitrogen losses and improving NUE. Future research should focus on optimizing the composition and assessing field-scale effectiveness to maximize its environmental and agronomic benefits.

Supplementary Information

The online version contains supplementary material available at https://doi.org/10.1007/s42773-025-00516-5.

Additional file 1.

Author contributions

Lan Luo: Data curation, Writing—original draft. Jie Li: Writing – review & editing, Conceptualization, Supervision. Anina James: Validation, Writing – review & editing. Caixia Hu: Measurement, Data curation, Software. Guilong Zhang: Conceptualization, Supervision, Validation, Funding acquisition, Writing—review & editing. Junting Pan: Conceptualization, Supervision, Validation, Funding acquisition, Writing—review & editing. All authors read and approved the final manuscript.

Funding

This study was financially supported by National Key R&D Program of China (2023YFD1701800, 2023YFD1701803), and the Chinese Academy of Agricultural Sciences Innovation Program.

Data availability

The datasets used or analyzed during the current study are available from the corresponding author upon reasonable request.

Declarations

Competing interests

The authors declare that they have no known competing financial interests or personal relationships that could have appeared to influence the work reported in this paper.

Author details

[1]Agro-Environmental Protection Institute, Ministry of Agriculture and Rural Affairs, Tianjin 300191, China. [2]State Key Laboratory of Efficient Utilization of Arable Land in China, Institute of Agricultural Resources and Regional Planning, Chinese Academy of Agricultural Sciences, Beijing 100081, China.

Received: 14 April 2025 Revised: 3 September 2025 Accepted: 8 September 2025
Published online: 07 November 2025

References

Afzal MTK, Firouzi AF, Zahedkolaei MT (2024) Enhanced transport of zerovalent iron nanoparticles and nitrate removal in saturated porous media. Water Air Soil Pollut 235:548–567. https://doi.org/10.1007/s11270-024-07361-5

Alami NE, Bourguid M, Kouighat M (2025) Advances in nitrogen use efficiency of ^{15}N-enriched fertilizers: a thirty-year review of research and innovations for sustainable agriculture. J Soil Sci Plant Nutr 1:1–23. https://doi.org/10.1007/s42729-025-02458-0

Amin FR, Huang Y, He Y, Zhang R, Liu G, Chen C (2016) Biochar applications and modern techniques for characterization. Clean Technol Environ Policy 18:1457–1473. https://doi.org/10.1007/s10098-016-1218-8

Awang NA, Wan Salleh WN, Aziz F, Yusof N, Ismail AF (2023) A review on preparation, surface enhancement and adsorption mechanism of biochar-supported nano zero-valent iron adsorbent for hazardous heavy metals. J Chem Technol Biotechnol 98(1):22–44. https://doi.org/10.1002/jctb.7182

Bae W, Kim S, Lee J, Chung J (2019) Effect of leachate circulation with ex situ nitrification on waste decomposition and nitrogen removal for early stabilization of fresh refuse landfill. J Hazard Mater 371:721–727. https://doi.org/10.1016/j.jhazmat.2019.03.058

Cai R, Wang X, Ji X, Peng B, Tan C, Huang X (2017) Phosphate reclaim from simulated and real eutrophic water by magnetic biochar derived from water hyacinth. J Environ Manage 187:212–219. https://doi.org/10.1016/j.jenvman.2016.11.047

Cao H, Ning L, Xun M, Feng F, Li P, Yue S, Song J, Zhang W, Yang H (2019) Biochar can increase nitrogen use efficiency of *Malus hupehensis* by modulating nitrate reduction of soil and root. Appl Soil Ecol 135:25–32. https://doi.org/10.1016/j.apsoil.2018.11.002

Chandra S, Medha I, Bhattacharya J (2020) Potassium-iron rice straw biochar composite for sorption of nitrate, phosphate, and ammonium ions in soil for timely and controlled release. Sci Total Environ 712:136337. https://doi.org/10.1016/j.scitotenv.2019.136337

Chen D, Suter HC, Islam A, Edis R (2010) Influence of nitrification inhibitors on nitrification and nitrous oxide (N_2O) emission from a clay loam soil fertilized with urea. Soil Biol Biochem 42(4):660–664. https://doi.org/10.1016/j.soilbio.2009.12.014

Chen C, Yang F, Ma Y, Dai L, Zhang Z, Guo H, Ding Y (2024) Ball milling boosted magnetic cotton husk-derived biochar adsorptive removal of oxytetracycline and ciprofloxacin from water. Carbon Res 3:63–76. https://doi.org/10.1007/s44246-024-00146-9

Cybulak M, Sokołowska Z, Boguta P (2021) The influence of biochar on the content of carbon and the chemical transformations of fallow and grassland humic acids. Sci Rep 11:5698–5712. https://doi.org/10.1038/s41598-021-85239-w

Dewage NB, Liyanage AS, Pittman CU Jr, Mohan D, Mlsna T (2018) Fast nitrate and fluoride adsorption and magnetic separation from water on α-Fe_2O_3 and Fe_3O_4 dispersed on Douglas fir biochar. Bioresour Technol 263:258–265. https://doi.org/10.1016/j.biortech.2018.05.001

Dissanayaka Mudiyanselage T, Franks A, Xu J, Bolan N, Wang H, Tang C (2020) Chemical and biological immobilization mechanisms of potentially toxic elements in biochar-amended soils. Crit Rev Environ Sci Technol 50(9):903–978. https://doi.org/10.1080/10643389.2019.1642832

Dong Y, Li Y, Kong F, Zhang J, Xi M (2020) Source, structural characteristics and ecological indication of dissolved organic matter extracted from sediments in the primary tributaries of the Dagu River. Ecol Indic 109:105776. https://doi.org/10.1016/j.ecolind.2019.105776

Fan Y, Sun S, Gu X, Yan P, Zhang Y, Peng Y, He S (2025) Tracing the electron transfer behavior driven by hydrophyte-derived carbon materials empowered autotrophic denitrification in iron-based constructed wetlands: efficacy and enhancement mechanism. Water Res 275:123169. https://doi.org/10.1016/j.watres.2025.123169

Gao C, Lu Y, Wang Y, Wang C, Hübner R, Li Y, Zhan J, Zhao M, Cai B (2022) Tuning iron-oxygen covalency in perovskite oxides for efficient electrochemical sensing. J Phys Chem C 126(41):17618–17626. https://doi.org/10.1021/acs.jpcc.2c06109

Gillingham MD, Gomes RL, Ferrari R, West HM (2022) Sorption, separation and recycling of ammonium in agricultural soils: a viable application for magnetic biochar? Sci Total Environ 812:151440. https://doi.org/10.1016/j.scitotenv.2021.151440

Guo JH, Liu XJ, Zhang Y, Shen J, Han W, Zhang W, Christie P, Goulding K, Vitousek P, Zhang F (2010) Significant acidification in major Chinese croplands. Science 327:1008–1010. https://doi.org/10.1126/science.1182570

Guo X, Yang Z, Liu H, Lv X, Tu Q, Ren Q, Xia X, Jing C (2015) Common oxidants activate the reactivity of zero-valent iron (ZVI) and hence remarkably enhance nitrate reduction from water. Sep Purif Technol 146:227–234. https://doi.org/10.1016/j.seppur.2015.03.059

Guo Z, Wang D, Yan Z, Qian L, Yang L, Yan J, Chen M (2023) Efficient remediation of p-chloroaniline contaminated soil by activated persulfate using ball milling nanosized zero valent iron/biochar composite: performance and mechanisms. Nanomater 13(9):1517–1533. https://doi.org/10.3390/nano13091517

He Y, Lin H, Dong Y, Li B, Wang L, Chu S, Luo M, Liu J (2018) Zeolite supported Fe/Ni bimetallic nanoparticles for simultaneous removal of nitrate and phosphate: synergistic effect and mechanism. Chem Eng J 347:669–681. https://doi.org/10.1016/j.cej.2018.04.088

Hei S, Xu H, Liu B, Zhu X, Zhang S, Zhang X, Li R, Huang X (2022) Enhanced pre-treatment of sepiolite on coal gasification wastewater: performance and adsorption mechanism. J Hazard Mater 440:129842. https://doi.org/10.1016/j.jhazmat.2022.129842

Heydari H, Raissi H, Ghahari A (2024) Engineered crystalline polymers for effective contaminant removal from water. Sci Rep 14:31869. https://doi.org/10.1038/s41598-024-83192-y

Hossain MZ, Bahar MM, Sarkar B, Donne SW, Ok YS, Palansooriya KN, Kirkham MB, Chowdhury S, Bolan N (2020) Biochar and its importance on nutrient dynamics in soil and plant. Biochar 2:379–420. https://doi.org/10.1007/s42773-020-00065-z

Hu X, Xu J, Wu M, Xing J, Bi W, Wang K, Ma J, Liu XE (2017) Effects of biomass pre-pyrolysis and pyrolysis temperature on magnetic biochar properties. J Anal Appl Pyrolysis 127:196–202. https://doi.org/10.1016/j.jaap.2017.08.006

Huang J, Jones A, Waite TD, Chen Y, Huang X, Rosso KM, Kappler A, Mansor M, Tratnyek PG, Zhang H (2021) Fe (II) redox chemistry in the environment. Chem Rev 121(13):8161–8233. https://doi.org/10.1021/acs.chemrev.0c01286

Jin Z, Chen X, Chen C, Tao P, Han Z, Zhang X (2016) Biochar impact on nitrate leaching in upland red soil, China. Environ Earth Sci 75:1109–1119. https://doi.org/10.1007/s12665-016-5906-9

Kim K, Baltus RE, Chellam S (2023) Rejection and fouling of track-etched microfiltration membranes by Acholeplasma laidlawii: Clues to mycoplasma behavior during "sterile" dead-end filtration. J Membr Sci 685:121925. https://doi.org/10.1016/j.memsci.2023.121925

Kong Q, Shi X, Ma W, Zhang F, Yu T, Zhao F, Zhao D, Wei C (2021) Strategies to improve the adsorption properties of graphene-based adsorbent towards heavy metal ions and their compound pollutants: a review. J Hazard Mater 415:125690. https://doi.org/10.1016/j.jhazmat.2021.125690

Li H, Yao R, Gao Q, Liu Y, Yang J, Wang X, Xie W, Zhang X (2023) Nanoattapulgite reduces the stimulation effect of nitrogen fertilizer on ammonia-oxidizing microorganisms in salinized fluvo-aquic soil. Land Degrad Dev 34(12):3475–3486. https://doi.org/10.1002/ldr.4696

Li C, Hu Y, Yan C, Zhang Y, Fan Y, Ji D, Wang B, Zhu L (2024) Biochar supported modified nZVI for effective remediation of hexavalent chromium: enhanced performance and remediation mechanism. J Environ Chem Eng 12(6):114410. https://doi.org/10.1016/j.jece.2024.114410

Liu Y, Wang J (2019) Reduction of nitrate by zero valent iron (ZVI)-based materials: a review. Sci Total Environ 671:388–403. https://doi.org/10.1016/j.scitotenv.2019.03.317

Liu B, Liu Z, Wu H, Pan S, Cheng X, Sun Y, Xu Y (2020a) Effective and simultaneous removal of organic/inorganic arsenic using polymer-based hydrated iron oxide adsorbent: capacity evaluation and mechanism. Sci Total Environ 742:140508. https://doi.org/10.1016/j.scitotenv.2020.140508

Liu J, Jiang J, Meng Y, Aihemaiti A, Xu Y, Xiang H, Gao Y, Chen X (2020b) Preparation, environmental application and prospect of biochar-supported metal nanoparticles: a review. J Hazard Mater 388:122026. https://doi.org/10.1016/j.jhazmat.2020.122026

Liu B, Li H, Li H, Zhang A, Rengel Z (2021) Long-term biochar application promotes rice productivity by regulating root dynamic development and reducing nitrogen leaching. GCB Bioenergy 13(1):257–268. https://doi.org/10.1111/gcbb.12766

Liu A, Ma X, Zhang Z, Liu J, Luo D, Yang L, Lv N, Zhang Y, Yang G, Dong H (2022a) Single dose fertilization at reduced nitrogen rate improves nitrogen utilization without yield reduction in late-planted cotton under a wheat–cotton cropping system. Ind Crops Prod 176:114346. https://doi.org/10.1016/j.indcrop.2021.114346

Liu G, Dai Z, Liu X, Dahlgren RA, Xu J (2022b) Modification of agricultural wastes to improve sorption capacities for pollutant removal from water—a review. Carbon Res 1:24–48. https://doi.org/10.1007/s44246-022-00025-1

Liu M, Chen G, Xu L, He Z, Ye Y (2024) Environmental remediation approaches by nanoscale zero valent iron (nZVI) based on its reductivity: a review. RSC Adv 14:21118–21138. https://doi.org/10.1039/D4RA02789B

Liu M, Xu X, Wanek W, Sun J, Bardgett RD, Tian Y, Cui X, Jiang L, Ma Z, Kuzyakov Y, Ouyang H, Wang Y (2025) Nitrogen availability in soil controls uptake of different nitrogen forms by plants. New Phytol 245(4):1450–1467. https://doi.org/10.1111/nph.20335

Ma F, Zhao B, Diao J, Jiang Y, Zhang J (2020) Mechanism of phosphate removal from aqueous solutions by biochar supported nanoscale zero-valent iron. RSC Adv 10:39217–39225. https://doi.org/10.1039/D0RA07391A

Ma D, Yang Y, Liu B, Xie G, Chen C, Ren N, Xing D (2021) Zero-valent iron and biochar composite with high specific surface area via K_2FeO_4 fabrication enhances sulfadiazine removal by persulfate activation. Chem Eng J 408:127992. https://doi.org/10.1016/j.cej.2020.127992

Meng Z, Huang S, Xu T, Lin Z, Wu J (2022) Competitive adsorption, immobilization, and desorption risks of Cd, Ni, and Cu in saturated-unsaturated soils by biochar under combined aging. J Hazard Mater 434:128903. https://doi.org/10.1016/j.jhazmat.2022.128903

Mokete R, Eljamal O, Sugihara Y (2020) Exploration of the reactivity of nanoscale zero-valent iron (NZVI) associated nanoparticles in diverse experimental conditions. Chem Eng Process 150:107879. https://doi.org/10.1016/j.cep.2020.107879

Noda I, Ozaki Y (2004) Two-dimensional correlation spectroscopy: applications in vibrational and optical spectroscopy. Wiley, London

Pei Y, Cheng W, Liu R, Di H, Jiang Y, Zheng C, Jiang Z (2024) Synergistic effect and mechanism of nZVI/LDH composites adsorption coupled reduction of nitrate in micro-polluted water. J Hazard Mater 464:133023. https://doi.org/10.1016/j.jhazmat.2023.133023

Perveen S, Nadeem R, Iqbal M, Bibi S, Gill R, Saeed R, Noreen S, Akhtar K, Ansari TM, Alfryyan N (2021) Graphene oxide and Fe_3O_4 composite synthesis, characterization and adsorption efficiency evaluation for NO_3^- and PO_4^{3-} ions in aqueous medium. J Mol Liq 339:116746. https://doi.org/10.1016/j.molliq.2021.116746

Qiao C, Liu L, Hu S, Compton JE, Greaver TL, Li Q (2015) How inhibiting nitrification affects nitrogen cycle and reduces environmental impacts of anthropogenic nitrogen input. Glob Change Biol 21(3):1249–1257. https://doi.org/10.1111/gcb.12802

Qiu B, Shao Q, Shi J, Yang C, Chu H (2022) Application of biochar for the adsorption of organic pollutants from wastewater: modification strategies, mechanisms and challenges. Sep Purif Technol 300:121925. https://doi.org/10.1016/j.seppur.2022.121925

Rushimisha IE, Li X, Han T, Chen X, Abdoul Magid ASI, Sun Y, Li Y (2024) Application of biochar on soil bioelectrochemical remediation: behind roles, progress, and potential. Crit Rev Biotechnol 44(1):120–138. https://doi.org/10.1080/07388551.2022.2119547

Sonal S, Mishra BK (2021) A comprehensive review on the synthesis and performance of different zirconium-based adsorbents for the removal of various water contaminants. Chem Eng J 424:130509. https://doi.org/10.1016/j.cej.2021.130509

Su JZ, Wang CC, Zhang MY, Zong XB, Huang XF, Deng ZH, Xiang P (2023) Advances and prospectives of iron/biochar composites: application, influencing factors and characterization methods. Ind Crops Prod 205:117496. https://doi.org/10.1016/j.indcrop.2023.117496

Sun Y, Gao B, Yao Y, Fang J, Zhang M, Zhou Y, Chen H, Yang L (2014) Effects of feedstock type, production method, and pyrolysis temperature on biochar and hydrochar properties. Chem Eng J 240:574–578. https://doi.org/10.1016/j.cej.2013.10.081

Tan XF, Zhu SS, Wang RP, Chen YD, Show PL, Zhang FF, Ho SH (2021) Role of biochar surface characteristics in the adsorption of aromatic compounds: pore structure and functional groups. Chin Chem Lett 32(10):2939–2946. https://doi.org/10.1016/j.cclet.2021.04.059

Tang TT, Xing QJ, Zhang SH, Mu Y, Jiang XH, Zhou ZG, Xiao X, Zou JP (2019) High selective reduction of nitrate into nitrogen by novel Fe-Cu/D407 composite with excellent stability and activity. Environ Pollut 252:888–896. https://doi.org/10.1016/j.envpol.2019.05.071

Tang H, Wang J, Zhang S, Pang H, Wang X, Chen Z, Li M, Song G, Qiu M, Yu S (2021) Recent advances in nanoscale zero-valent iron-based materials: characteristics, environmental remediation and challenges. J Clean Prod 319:128641. https://doi.org/10.1016/j.jclepro.2021.128641

Tran HN, Lima EC, Juang RS, Bollinger JC, Chao HP (2021) Thermodynamic parameters of liquid–phase adsorption process calculated from different equilibrium constants related to adsorption isotherms: a comparison study. J Environ Chem Eng 9(6):106674. https://doi.org/10.1016/j.jece.2021.106674

Tu W, Liu Y, Xie Z, Chen M, Ma L, Du G, Zhu M (2021) A novel activation-hydrochar via hydrothermal carbonization and KOH activation of sewage sludge and coconut shell for biomass wastes: preparation, characterization and adsorption properties. J Colloid Interface Sci 593:390–407. https://doi.org/10.1016/j.jcis.2021.02.133

Wan X, Li C, Parikh SJ (2020) Simultaneous removal of arsenic, cadmium, and lead from soil by iron-modified magnetic biochar. Environ Pollut 261:114157. https://doi.org/10.1016/j.envpol.2020.114157

Wang H, Gao JE, Li XH, Zhang SL, Wang HJ (2015) Nitrate accumulation and leaching in surface and ground water based on simulated rainfall experiments. PLoS ONE 10(8):e0136274. https://doi.org/10.1371/journal.pone.0136274

Wang S, Zhao M, Zhou M, Li YC, Wang J, Gao B, Sato S, Feng K, Yin W, Igalavithana AD (2019) Biochar-supported nZVI (nZVI/BC) for contaminant removal from soil and water: a critical review. J Hazard Mater 373:820–834. https://doi.org/10.1016/j.jhazmat.2019.03.080

Wang Y, Wang Z, Pang WK, Lie W, Yuwono JA, Liang G, Liu S, Angelo AMD, Deng J, Fan Y (2023) Solvent control of water O—H bonds for highly reversible zinc ion batteries. Nat Commun 14:2720–2731. https://doi.org/10.1038/s41467-023-38384-x

Wei A, Ma J, Chen J, Zhang Y, Song J, Yu X (2018) Enhanced nitrate removal and high selectivity towards dinitrogen for groundwater remediation using biochar-supported nano zero-valent iron. Chem Eng J 353:595–605. https://doi.org/10.1016/j.cej.2018.07.127

Wu P, Fu Y, Vancov T, Wang H, Wang Y, Chen W (2024a) Analyzing the trends and hotspots of biochar's applications in agriculture, environment, and energy: a bibliometrics study for 2022 and 2023. Biochar 6:78–96. https://doi.org/10.1007/s42773-024-00370-x

Xu W, Huang D, Wang G, Li S, Du L, Zhou W, Huang H (2024a) Enhanced sulfamethazine degradation via peroxydisulfate activation by biochar-supported nano zero-valent iron-copper: the key role of Fe (IV) and electron transfer induced by doped Cu. J Clean Prod 434:140133. https://doi.org/10.1016/j.jclepro.2023.140133

Xu Y, Zanli BLGL, Chen J (2024b) New consideration on the application of nano-zero-valent iron (nZVI) in groundwater remediation: refractions to existing technologies. J Nanopart Res 26:11–35. https://doi.org/10.1007/s11051-023-05919-8

Yan P, Li T, Ren T, Zang Y, Sun S, Fan Y, Zhang Y, Gu X, He S (2025) Heterotrophic denitrification enhancement via effective organic matter degradation driven by suitable iron dosage in sediment. J Environ Manage 375:124275. https://doi.org/10.1016/j.jenvman.2025.124275

Yi Y, Tu G, Zhao D, Tsang PE, Fang Z (2019) Biomass waste components significantly influence the removal of Cr (VI) using magnetic biochar derived

from four types of feedstocks and steel pickling waste liquor. Chem Eng J 360:212–220. https://doi.org/10.1016/j.cej.2018.11.205
Yuan Y, Wei X, Yin H, Zhu M, Luo H, Dang Z (2022) Synergistic removal of Cr (VI) by S-nZVI and organic acids: the enhanced electron selectivity and pH-dependent promotion mechanisms. J Hazard Mater 423:127240. https://doi.org/10.1016/j.jhazmat.2021.127240
Yuan T, Tai AP, Mao J, Tam OH, Li RK, Wu J, Li S (2023) Effects of different irrigation methods on regional climate in North China Plain: a modeling study. Agric for Meteorol 342:109728. https://doi.org/10.1016/j.agrformet.2023.109728
Zhang M, Song G, Gelardi DL, Huang L, Khan E, Mašek O, Parikh SJ, Ok YS (2020) Evaluating biochar and its modifications for the removal of ammonium, nitrate, and phosphate in water. Water Res 186:116303. https://doi.org/10.1016/j.watres.2020.116303
Zhang Z, Huang G, Zhang P, Shen J, Wang S, Li Y (2023a) Development of iron-based biochar for enhancing nitrate adsorption: effects of specific surface area, electrostatic force, and functional groups. Sci Total Environ 856:159037. https://doi.org/10.1016/j.scitotenv.2022.159037
Zhang Y, Bi Z, Tian W, Ge Z, Xu Y, Xu R, Zhang H, Tang S (2023b) Synergistic effect triggered by Fe_2O_3 and oxygen-induced hydroxyl radical enhances formation of amino-phenolic humic-like substance. J Environ Manage 348:119312. https://doi.org/10.1016/j.jenvman.2023.119312
Zhang M, Wang L, Zhao Q, Wang J, Sun Y (2024) Hydrogeochemical and anthropogenic controls on quality and quantitative source-specific risks of groundwater in a resource-based area with intensive industrial and agricultural activities. J Cleaner Prod 440:140911. https://doi.org/10.1016/j.jclepro.2024.140911
Zhao X, Yu G, Li J, Feng Y, Zhang L, Peng Y, Tang Y, Wang L (2018) Eco-friendly Pickering emulsion stabilized by silica nanoparticles dispersed with high-molecular-weight amphiphilic alginate derivatives. ACS Sustain Chem Eng 6(3):4105–4114. https://doi.org/10.1021/acssuschemeng.7b04508
Zhao F, Xin J, Yuan M, Wang L, Wang X (2022) A critical review of existing mechanisms and strategies to enhance N_2 selectivity in groundwater nitrate reduction. Water Res 209:117889. https://doi.org/10.1016/j.watres.2021.117889
Zhao X, Wang Q, Sun Y, Li H, Lei Z, Zheng B, Xia H, Su Y, Ali KMY, Wang H (2024) Beryllium adsorption from beryllium mining wastewater with novel porous lotus leaf biochar modified with PO_4^{3-}/NH_4^+ multi-functional groups (MLLB). Biochar 6:89–103. https://doi.org/10.1007/s42773-024-00385-4
Zhu X, Zhou P, Miao P, Wang H, Bai X, Chen Z, Zhou J (2022) Nitrogen use and management in orchards and vegetable fields in china: challenges and solutions. Front Agr Sci Eng 9(3):386–395. https://doi.org/10.15302/J-FASE-2022443